Analog of Rabi oscillations in resonant electron-ion systems

Lorenzo Stella,[1, 2, a)] Rafael P. Miranda,[1, 2] Andrew P. Horsfield,[3] and Andrew J. Fisher[1, 2]

[1)] *Department of Physics and Astronomy, University College London, Gower Street, London WC1E 6BT, United Kingdom*

[2)] *London Centre for Nanotechnology, 17–19 Gordon Street, London WC1H 0AH, United Kingdom*

[3)] *Department of Materials, Imperial College London, South Kensington Campus, London SW7 2AZ, United Kingdom*

Quantum coherence between electron and ion dynamics, observed in organic semiconductors by means of ultrafast spectroscopy, is the object of recent theoretical and computational studies. To simulate this kind of quantum coherent dynamics, we have introduced in a previous article (J. Chem. Phys. **127**, 214104 (2007)) an improved computational scheme based on Correlated Electron-Ion Dynamics (CEID). In this article, we provide a generalization of that scheme to model several ionic degrees of freedom and many-body electronic states. To illustrate the capability of this extended CEID, we study a model system which displays the electron-ion analog of the Rabi oscillations. Finally, we discuss convergence and scaling properties of the extended CEID along with its applicability to more realistic problems.

PACS numbers: 31.15.Qg, 31.50.Gh

[a)] Current affiliation: Nano-Bio Spectroscopy group and ETSF Scientific Development Centre, Dpto. Física de Materiales, Universidad del País Vasco, Centro de Física de Materiales CSIC-UPV/EHU-MPC and DIPC, Av. Tolosa 72, E-20018 San Sebastián, Spain; Electronic mail: lorenzo.stella@ehu.es

I.   INTRODUCTION

Many technologically relevant[1] molecular materials—and in particular organic semiconductors—display an enhanced coupling between electronic transitions and molecular oscillations,[2] i.e., nonadiabatic coupling. This class of compounds has been often modeled by semiempirical Hamiltonians[3] like the Pariser-Parr-Pople Hamiltonian and its derivatives.[4] In the case of π-conjugated polymers, even the simpler Su-Schrieffer-Heeger (SSH) Hamiltonian[5] can be used to study the dynamical features caused by the strong nonadiabatic coupling.[6]

Including electronic transitions and—possibly classical—atomic motion in a consistent[7,8] and computationally effective molecular dynamics scheme has been the object of intense theoretical and computational investigations during the last decades.[9–19]

In the surface hopping algorithm[10]—and similar approaches[12,14,18] that treat atomic evolution classically—vertical electronic transitions are included in a stochastic way. By averaging over a large ensemble of such stochastic quantum-classical evolutions, one obtains a reliable approximation to the quantum electron-ion[20] dynamics. Efficient surface hopping algorithms make use of adiabatic electronic states in order to minimize the number of hops attempted during the simulation.[11,12] However, working with adiabatic electronic states requires the diagonalization of the electronic Hamiltonian at each molecular dynamics time step, which is a costly numerical operation.

Ehrenfest Dynamics (ED)[11,17,19] is a very efficient deterministic quantum-classical evolution which requires neither ensemble averages nor adiabatic electronic states. On the other hand, ED is known to miss part of the quantum electron-ion correlation[8,15,16] which turns out to be crucial in nonequilibrium conditions.[21]

Methods based on ionic wave functions, e.g., *ab initio* multiple-spawning,[13] have been also investigated, since they include quantum features of the ion dynamics which are not accounted for by any quantum-classical evolution. Nevertheless, as in the case of surface hopping, these methods are effective for gas phase simulations[22] when a relatively small number of spawning events is expected.

For condensed phase simulations—and in particular for metallic systems—methods based on smooth equations of motion (EOMs) for the combined electron-ion evolution as ED and its generalizations[15,16,23,24] are usually preferred.

Dynamics in condensed and gas phases also differ because of the role quantum electron-

ion coherence can possibly play. In the gas phase, atoms interact only briefly before leaving the collision region, while in condensed phases—and especially at low dimensions—multiple, periodic interactions, e.g., due to steady molecular oscillations, can build up quantum coherence between electrons and ions.[25] There is also increasing evidence that quantum electron-ion coherence can play a role in photosynthesis[26] and in the nonradiative relaxation of π-conjugated polymers, even at room temperature.[27]

Recent theoretical and computational investigations by means of effective kinetic equations for the electronic degrees of freedom (DOFs)[28] have demonstrated the subtle interplay between coherent (wave-like) and incoherent (thermal diffusion) dynamics. In this article we pursue a different approach to quantum electron-ion coherence, i.e., we simulate explicitly also the ionic DOFs by means of an extension of the CEID algorithm introduced in Ref. 23.

The extended CEID algorithm considered in this article is based on a perturbative—and systematically convergent—expansion of the quantum fluctuations of the ions about their Ehrenfest trajectory in phase space. This scheme shares similarities with the hierarchical electron-phonon model of Tamura et $al.$[29], although they use a different perturbation scheme by partitioning high and low frequency modes of the system.

The rest of this article is organized as follows: In Sec. II we show how to extend the CEID scheme of Ref. 23 to the many-atom case. In Sec. III we derive accurate initial conditions for the extended CEID algorithm. In Sec. IV we discuss a consistent way to include electronic structure calculations in the extended CEID algorithm. In Sec. V we illustrate the capabilities of the extended CEID algorithm by simulating a model system which shows the electron-ion analog of Rabi oscillations. Finally, in Sec. VI we provide a summary of the results presented and discuss the applicability of the extended CEID algorithm to more realistic problems, e.g., the nonradiative relaxation of π-conjugated polymers.[30]

II.   CEID FORMALISM FOR MANY-ATOM SYSTEMS

The CEID formalism has been introduced in previous articles[15,16,23,24] and in particular Ref. 23 contains a detailed derivation of the CEID EOMs for a system with one ionic DOF, e.g., a diatomic molecule in one dimension. In this Section we generalize that derivation to the many-atom case, namely N_I atoms (or ions) in D dimensions.

In the rest of this article we shall use P and R for the ionic momenta and positions,

and p and r for the correspondent electronic DOFs. Particle and coordinate indices will be employed only if directly addressed in calculation, otherwise a compact vectorial notation will be used, e.g., $P = (P_1, P_2, \ldots P_{DN_I})$, where the first D vector entries are the coordinates of the first ion and so forth. As usual, quantum momenta and positions will be distinguished from the corresponding classical observables by using the hat, e.g., $\hat{P}$.

A.   Adiabatic and nonadiabatic dynamics

The total electron-ion Hamiltonian is given by

$$H = \sum_{\alpha=1}^{N_I} \frac{\hat{P}_\alpha^2}{2M_\alpha} + H_e(\hat{R}) , \tag{1}$$

where we have employed the customary partition between kinetic energy of the ions and electronic Hamiltonian H_e.[10] The adiabatic *many-body* electronic states are obtained by diagonalizing H_e after the quantum operators $\hat{R}$ have been substituted by classical parameters, R:

$$H_e \Phi_n(r; R) = E_n(R) \Phi_n(r; R) , \tag{2}$$

where the nth eigenvalue, $E_n(R)$, as a function of R defines the nth adiabatic Potential Energy Surface (PES) of the system. [The eigenvectors are assumed to be orthonormalized.]

The instantaneous electronic wave function can be expanded in terms of the instantaneous adiabatic states as

$$\Phi(r, t) = \sum_n c_n(t) \Phi_n(r; R(t)) . \tag{3}$$

The mixed quantum-classical dynamics is said to be adiabatic if $\Phi(r, t) \simeq \Phi_n(r; R(t))$, i.e., if just one term on the R.H.S. of Eq. 3 is relevant. In this case, one defines the Born-Oppenheimer (BO)[31] Hamiltonian of the ions evolving on the nth adiabatic PES as

$$H_{bo}^{(n)} = \langle \Phi_n | H | \Phi_n \rangle = \sum_{\alpha=1}^{N_I} \frac{\hat{P}_\alpha^2}{2M_\alpha} + E_n(\hat{R}) . \tag{4}$$

By assuming classical ions, one can write the (conservative) adiabatic forces acting on the ions as

$$F_\alpha^{(n)} = -\frac{\partial E_n}{\partial R_\alpha} . \tag{5}$$

If these adiabatic forces are zero, i.e., in the adiabatic equilibrium configuration of the ions, one can also compute the adiabatic Hessian,

$$K_{\alpha,\beta}^{(n)} = \frac{\partial^2 E_n}{\partial R_\alpha \partial R_\beta} \; , \tag{6}$$

to obtain the adiabatic vibrational frequencies.

This adiabatic picture for classical ions breaks down when: i) The quantum nature of ions cannot be neglected, e.g., at low temperature. ii) Electronic transitions between adiabatic states occur, e.g., during the nonradiative relaxation of photoexcited molecules. In the nonadiabatic case, the following definitions of the average forces and Hessian apply:

$$\bar{F}_\alpha = -\mathrm{Tr}\left\{\rho \frac{\partial H_e}{\partial R_\alpha}\right\} \overset{\mathrm{def}}{=} \mathrm{Tr}\{\rho F_\alpha\} \tag{7}$$

and

$$\bar{K}_{\alpha,\beta} = \mathrm{Tr}\left\{\rho \frac{\partial^2 H_e}{\partial R_\alpha \partial R_\beta}\right\} \overset{\mathrm{def}}{=} \mathrm{Tr}\{\rho K_{\alpha,\beta}\} \; , \tag{8}$$

where ρ is the total—i.e., for electrons and ions—density matrix. The trace here is meant with respect to both electronic and ionic DOFs and the bar indicates a quantum mechanical average.

B. Ehrenfest dynamics

Thanks to the Ehrenfest theorem,[32] one can write down the *exact* EOMs for the average momenta $\bar{P} = \mathrm{Tr}\{\rho \hat{P}\}$ and positions $\bar{R} = \mathrm{Tr}\{\rho \hat{R}\}$:

$$\dot{\bar{P}}_\alpha = \bar{F}_\alpha \; , \tag{9a}$$

$$\dot{\bar{R}}_\alpha = \bar{P}_\alpha / M_\alpha \; . \tag{9b}$$

On the other hand, in order to compute the average forces, $\bar{F}_\alpha$, an explicit integration (trace) over *all* the DOFs must be done. The computational cost of this numerical integration scales very unfavorably (exponentially) with the number of ions, N_I.

In ED[11] two approximations are made to make the computation of the average forces affordable: i) The total density is assumed to be factorized

$$\rho = \rho_e \otimes \rho_I \; , \tag{10}$$

where ρ_e is the electronic density matrix and ρ_I is the ionic density matrix. [In general, $\rho_e = \mathrm{Tr}_I\{\rho\}$ and $\rho_I = \mathrm{Tr}_e\{\rho\}$, where Tr_I and Tr_e are the traces with respect to the ionic and

electronic DOFs, respectively.] ii) The ions are assumed to be classical, i.e., their density matrix describes an infinitely localized state in $R = \bar{R}$. As a consequence of these two approximations, the average ED forces read:

$$\bar{F}_\alpha^{(ed)} = \text{Tr}_e\{\rho_e F_\alpha(\bar{R})\} \ . \tag{11}$$

The missing EOM for ρ_e can be found by integrating out the ionic DOFs from the total Liouville equation

$$\frac{d\rho}{dt} = \frac{1}{\imath\hbar}[H, \rho] \tag{12}$$

using Eq. 10 and the approximation ii) stated above. The effective Liouville equation for the electronic density matrix is then:

$$\frac{d\rho_e}{dt} = \frac{1}{\imath\hbar}\left[H_e(\bar{R}), \rho_e\right] \ . \tag{13}$$

The combined propagation of Eq. 9 and Eq. 13 along with Eq. 11 conserves the Ehrenfest total energy:[11]

$$E_{tot}^{(ed)} = \sum_{\alpha=1}^{N_I} \frac{\bar{P}_\alpha^2}{2M_\alpha} + \text{Tr}_e\{\rho_e H_e(\bar{R})\} \ . \tag{14}$$

Although the total density matrix Eq. 10 is factorized, the electronic and ionic DOFs are correlated by the EOMs. On the other hand, part of the electron-ion correlation is missed by ED, leading in some cases to qualitatively wrong predictions.[8,10,21] Nevertheless, ED remains computationally appealing because it does not require the explicit knowledge of the adiabatic PESs, i.e., a costly diagonalization of H_e at each time-step is avoided. Therefore, in contrast with other schemes, ED can be employed to simulate large atomic systems,[19] including metals.[33]

C.   Representation of the quantum fluctuations of the ions

In order to get rid of an inessential mass dependence in the total Hamiltonian, Eq. 1, we perform the canonical transform

$$\begin{cases} \hat{P}_\alpha \rightarrow \hat{P}_\alpha\sqrt{M_\alpha/M_0} \ , \\ \hat{R}_\alpha \rightarrow \hat{R}_\alpha\sqrt{M_0/M_\alpha} \ , \end{cases} \tag{15}$$

where M_0 is some reference mass value, e.g., the average mass. We then introduce the operators that describe the quantum fluctuations of the ions as

$$
\begin{cases}
\Delta \hat{P}(t) = \hat{P} - \bar{P}(t) \,, \\
\Delta \hat{R}(t) = \hat{R} - \bar{R}(t) \,.
\end{cases}
\tag{16}
$$

According to Eq. 16, the quantum fluctuations of the ions follow the average phase flow given by the solution of the Ehrenfest EOMs, Eq. 9. This way one introduces a description of the quantum evolution of the ions analogous to the Lagrangian flow specification of fluid dynamics[34] (see Appendix A). This kind of description has to be contrasted with an Eulerian-like flow specification in which the quantum momentum and position operators are fixed with respect to an external reference frame, as in Eq. 15.

Due to the localized nature of the quantum fluctuations of the ions at low and moderate densities, a Lagrangian-like description is likely to be more appropriate than an Eulerian-like one in order to model the nonadiabatic dynamics of a molecular system.

Having formally defined the quantum fluctuations of the ions in Eq. 16, we expand the total Hamiltonian up to the second order with respect to $\Delta \hat{P}$ and $\Delta \hat{R}$:

$$
H \simeq \frac{1}{2M_0} \left[\sum_\alpha \bar{P}_\alpha^2 + 2 \sum_\alpha \bar{P}_\alpha \Delta \hat{P}_\alpha + \sum_\alpha \Delta \hat{P}_\alpha^2 \right] + H_e(\bar{R}) - \sum_\alpha F_\alpha(\bar{R}) \Delta \hat{R}_\alpha + \frac{1}{2} \sum_{\alpha,\beta} K_{\alpha,\beta}(\bar{R}) \Delta \hat{R}_\alpha \Delta \hat{R}_\beta \,.
\tag{17}
$$

We stopped at second-order because we found this approximation appropriate for the cases we have investigated so far.[23,30]

Eq. 17 is not equivalent to the harmonic expansion used to define phonons in solid state physics[35] because: i) In general $\bar{R}$ is not an equilibrium configuration. ii) The reference configuration (in phase space), $(\bar{P}(t), \bar{R}(t))$, is not fixed, but follows the phase flow given by the solution of the Ehrenfest EOMs, Eq. 9.

We apply the second quantization formalism[35] to the quantum fluctuations of the ions. This can be done in several unitarily equivalent ways—depending on the choice of the quantized modes—although some choices yield a more efficient numerical implementation than others (see Sec. III).

One can define a generic set of quantized modes starting from the original (or Cartesian)

$\Delta \hat{P}$ and $\Delta \hat{R}$ as

$$\begin{cases} \Delta \hat{\eta}_\alpha = \sum_\beta U_{\alpha,\beta} \Delta \hat{P}_\beta \ , \\ \Delta \hat{\zeta}_\alpha = \sum_\beta U^*_{\alpha,\beta} \Delta \hat{R}_\beta \ , \end{cases} \tag{18}$$

where U is a unitary operator. Then, we introduce for each quantized mode a pair of (bosonic) creation and annihilation operators, $a^\dagger$ and a[35] so that

$$\begin{cases} \Delta \hat{\eta}_\alpha = \frac{\imath}{\sqrt{2}} b_\alpha \left(a^\dagger_\alpha - a_\alpha \right) \ , \\ \Delta \hat{\zeta}_\alpha = \frac{1}{\sqrt{2}} a_\alpha \left(a^\dagger_\alpha + a_\alpha \right) \ . \end{cases} \tag{19}$$

The parameters a_α and b_α give $\Delta \hat{\zeta}_\alpha$ and $\Delta \hat{\eta}_\alpha$ the right dimensions. They are not independent, since $a_\alpha b_\alpha = \hbar$ must hold for all α in order to fulfill the canonical quantization rules $[\Delta \hat{R}_\alpha, \Delta \hat{P}_\beta] = \imath \hbar \delta_{\alpha,\beta} \mathbb{1}$.

In principle, there are $D N_I$ independent quantized modes. In practice, it is useful to introduce only quantum fluctuations of the ions along those $N_{coor} \leq D N_I$ quantized modes which are more strongly coupled with the electronic transitions. [One can use the definition of nonadiabatic coupling in Ref. 11.] We stress here that, even when a restricted number of quantized modes is included in the dynamics, we do not impose any constraint to the dynamics of $\bar{R}$ and $\bar{P}$ (apart from the boundary conditions).

In addition to the Cartesian modes, $\Delta \hat{P}$ and $\Delta \hat{R}$, a natural choice for the quantized modes are the eigenvectors of the initial average Hessian $\bar{K}_{\alpha,\beta}(t = 0)$, i.e., the normal (vibrational) modes of the initial configuration. However, since the average Hessian is time-dependent, it is not guaranteed that this initial choice will always correspond, even approximately, to the eigenvectors of the instantaneous average Hessian, $\bar{K}_{\alpha,\beta}(t)$.

It also worth noting that normal modes refer to a fixed equilibrium configuration, while the quantized modes refer to the evolving Ehrenfest trajectory in phase space (see Eq. 18 and Eq. 16).

D. Many-body ionic states

The vacuum or ground-state $|0\rangle$ represents the unavoidable zero-point quantum fluctuations of the ions about the Ehrenfest trajectory in phase space. A *many-body* basis set for the quantum fluctuations of the ions is then made by[35]

$$|n_1, n_2, \ldots\rangle = \prod_{i=1}^{N_{coor}} \frac{\left(a^\dagger_{\alpha_i} \right)^{n_i}}{\sqrt{(n_i)!}} |0\rangle \ , \tag{20}$$

i.e., the states in which the quantum fluctuations of the ions along quantized mode α_i have been excited n_i times. Note that, in contrast with phonons, states defined in Eq. 20 have an implicit time-dependence because they are defined with respect to an evolving Ehrenfest trajectory in phase space.

In the rest of the article, we shall use a compact vectorial notation for the occupation numbers, i.e., we shall write $|n\rangle$ instead of $|n_1, n_2, \ldots\rangle$. It is also useful to introduce a short-hand notation for many-body ionic states that differ from a reference state by a few quantum excitations. For instance, the state obtained by adding to $|n\rangle$ one quantum of fluctuation along the quantized mode α will be written as $|n + 1_\alpha\rangle \overset{\text{def}}{=} |n_1, \ldots, n_\alpha + 1, \ldots\rangle$. By means of this convention, the creation and annihilation operators read[35]

$$\begin{cases} a_\alpha^\dagger = \sum_n \sqrt{n_\alpha + 1}|n + 1_\alpha\rangle\langle n|, \\ a_\alpha = \sum_n \sqrt{n_\alpha}|n - 1_\alpha\rangle\langle n|. \end{cases} \tag{21}$$

Finally, we define the order of ionic many-body state $|n\rangle$ as $|n| = \sum_i n_i$ and $\mathcal{S}_{N_{ceid}}$ as the subset of the ionic Hilbert space generated by all the $|n\rangle$ with $|n| \leq N_{ceid}$. [In Appendix B we compute the linear dimension of $\mathcal{S}_{N_{ceid}}$ as a function of N_{ceid} and the number of quantized modes, N_{coor}.]

E.   Many-atom CEID expansion

Consider a generic Hermitian operator O, which in principle can depend on both ionic and electronic DOFs, e.g., the total Hamiltonian H or the total density matrix ρ. One can write an approximation of O by (partially) expanding with respect to the quantum fluctuations of the ions representable in $\mathcal{S}_{N_{ceid}}$, as

$$O \simeq O^{(N_{ceid})} = \sum_{n,m}|n\rangle O_{n,m}^{(N_{ceid})}(\bar{P}, \bar{R})\langle m| , \tag{22}$$

where

$$O_{n,m}^{(N_{ceid})}(\bar{P}, \bar{R}) = \begin{cases} \langle n|O|m\rangle & \text{if} \quad |n|, |m| \leq N_{ceid} \\ 0 & \text{otherwise} \end{cases} . \tag{23}$$

[In the rest of the paper we will omit the superscript (N_{ceid}) whenever the approximation is clear from the context.] Since Eq. 22 is a partial expansion, the matrix elements $O_{n,m}$ are not scalars, but electronic operators which depend on the instantaneous average momenta and positions, $\bar{P}, \bar{R}$.

By means of Eq. 18, Eq. 19, and Eq. 21, one can write down the matrix elements of the expanded Hamiltonian in Eq. 17 as

$$H_{n,m}\left(\bar{P}(\bar{\eta}), \bar{R}(\bar{\zeta})\right) = \frac{1}{2M_0}\sum_\alpha \bar{\eta}_\alpha^2 \delta_{m,n} - \frac{\imath}{\sqrt{2M_0}}\sum_\alpha b_\alpha \bar{\eta}_\alpha \left[\sqrt{m_\alpha}\delta_{m-1_\alpha,n} - \sqrt{n_\alpha}\delta_{m,n-1_\alpha}\right]$$

$$- \frac{1}{4M_0}\sum_\alpha b_\alpha^2 \left[\sqrt{m_\alpha(m_\alpha-1)}\delta_{m-2_\alpha,n} - (2m_\alpha+1)\delta_{m,n} + \sqrt{n_\alpha(n_\alpha-1)}\delta_{m,n-2_\alpha}\right]$$

$$+ H_e\left(\bar{\zeta}\right)\delta_{m,n} - \frac{1}{\sqrt{2}}\sum_\alpha a_\alpha \tilde{F}_\alpha\left(\bar{\zeta}\right)\left[\sqrt{m_\alpha}\delta_{m-1_\alpha,n} + \sqrt{n_\alpha}\delta_{m,n-1_\alpha}\right]$$

$$+ \frac{1}{4}\sum_\alpha a_\alpha^2 \tilde{K}_{\alpha,\alpha}\left(\bar{\zeta}\right)\left[\sqrt{m_\alpha(m_\alpha-1)}\delta_{m-2_\alpha,n} + (2m_\alpha+1)\delta_{m,n}\right.$$

$$\left. + \sqrt{n_\alpha(n_\alpha-1)}\delta_{m,n-2_\alpha}\right]$$

$$+ \frac{1}{2}\sum_{\alpha<\beta} a_\alpha a_\beta \tilde{K}_{\alpha,\beta}\left(\bar{\zeta}\right)\left[\sqrt{m_\alpha m_\beta}\delta_{m-1_\alpha-1_\beta,n} + \sqrt{m_\alpha n_\beta}\delta_{m-1_\alpha,n-1_\beta}\right.$$

$$\left. + \sqrt{n_\alpha m_\beta}\delta_{m-1_\beta,n-1_\alpha} + \sqrt{n_\alpha n_\beta}\delta_{m,n-1_\alpha-1_\beta}\right] ,$$

$$(24)$$

where $\bar{\eta}_\alpha = \sum_\beta U_{\alpha,\beta}\bar{P}_\beta$, $\bar{\zeta}_\alpha = \sum_\beta U^*_{\alpha,\beta}\bar{R}_\beta$ (see Eq. 18),

$$\tilde{F}_\alpha = \sum_\beta U^*_{\alpha,\beta}F_\beta , \tag{25}$$

and

$$\tilde{K}_{\alpha,\beta} = \sum_{\gamma,\delta} U^*_{\alpha,\gamma}K_{\gamma,\delta}U_{\delta,\beta} . \tag{26}$$

The final term of Eq. 24 contains the mixing of quantum fluctuations of the ions relative to different quantized modes. Since the matrix $\tilde{K}(\bar{\zeta})$ has an implicit time-dependence through $\bar{\zeta}$, in general it is not possible to get rid of the last two lines of Eq. 24 by a time-independent coordinate transform, as in Eq. 18.

Finally, by Eq. 22, the average forces defined in Eq. 7 can be approximated as[36]

$$\bar{F}_a = \sum_{|n|,|m|=0}^{N_{ceid}} \text{Tr}_e\left\{\rho_{n,m}\left(F_\alpha\right)_{m,n}\right\} , \tag{27}$$

which reduces to an expression similar to Eq. 11 if $N_{ceid} = 0$.

10

F. Many-atom CEID equations of motion

The many-body ionic basis set defined in Sec. II D is convenient to describe quantum fluctuations of ions very localized about their Ehrenfest trajectory in phase space. On the other hand, this choice makes this set implicitly time-dependent through its dependence on $\bar{P}$ and $\bar{R}$.

To simplify the derivation of the EOMs for the matrix coefficients of ρ, one can use a kind of Heisenberg picture[32] in which the basis set does not evolve and the operators acquire an implicit time-dependence through the extra dependence on $\bar{P}$ and $\bar{R}$ they get (see Appendix A). In this picture—analogous to the Lagrangian flow specification of fluid dynamics—the Liouville EOM reads (see Eq. A6)

$$\frac{\mathrm{d}\rho}{\mathrm{d}t} = \frac{1}{\imath\hbar}\left[H^{(mat)}, \rho\right] \tag{28}$$

where

$$H^{(mat)} = H + \sum_{\alpha} \bar{F}_{\alpha}\Delta\hat{R}_{\alpha} - \frac{\bar{P}_{\alpha}}{M_0}\Delta\hat{P}_{\alpha} \tag{29}$$

is the effective Hamiltonian operator for this flow specification.

One can now safely expand Eq. 28 according to Eq. 22 and Eq. 23 to obtain a set of approximate EOMs for the matrix elements of ρ:

$$\dot{\rho}_{n,m} = \frac{1}{\imath\hbar}\sum_{|k|=0}^{N_{ceid}}\left[H^{(mat)}_{n,k}\,\rho_{k,m} - \rho_{n,k}\,H^{(mat)}_{k,m}\right] \tag{30}$$

if $|n|, |m| \leq N_{ceid}$ and 0 otherwise.

Finally, by computing $H^{(mat)}_{n,m}$ as in Eq. 24 and plugging the result in Eq. 30, one obtains the CEID EOMs:

11

$$
\begin{aligned}
\dot{\rho}_{n,m} =\ & -\frac{1}{4M_0 \imath \hbar} \sum_\alpha b_\alpha^2 \left[\sqrt{(n_\alpha+2)(n_\alpha+1)}\rho_{n+2_\alpha,m} - (2n_\alpha+1)\rho_{n,m} + \sqrt{n_\alpha(n_\alpha-1)}\rho_{n-2_\alpha,m} \right. \\
& \left. -\sqrt{m_\alpha(m_\alpha-1)}\rho_{n,m-2_\alpha} + (2m_\alpha+1)\rho_{n,m} - \sqrt{(m_\alpha+2)(m_\alpha+1)}\rho_{n,m+2_\alpha} \right] + \frac{1}{\imath\hbar}\left[H_e(\bar\zeta),\rho_{n,m} \right] \\
& -\frac{1}{\sqrt{2}\imath\hbar} \sum_\alpha a_\alpha \left[\Delta\tilde{F}_\alpha(\bar\zeta)\left(\sqrt{n_\alpha+1}\rho_{n+1_\alpha,m} + \sqrt{n_\alpha}\rho_{n-1_\alpha,m} \right) - \left(\sqrt{m_\alpha}\rho_{n,m-1_\alpha} + \sqrt{m_\alpha+1}\rho_{n,m+1_\alpha} \right) \right. \\
& \left. \Delta\tilde{F}_\alpha(\bar\zeta) \right] \\
& +\frac{1}{4\imath\hbar} \sum_\alpha a_\alpha^2 \left[\tilde{K}_{\alpha,\alpha}(\bar\zeta)\left(\sqrt{(n_\alpha+2)(n_\alpha+1)}\rho_{n+2_\alpha,m} + (2n_\alpha+1)\rho_{n,m} + \sqrt{n_\alpha(n_\alpha-1)}\rho_{n-2_\alpha,m} \right) \right. \\
& \left. - \left(\sqrt{m_\alpha(m_\alpha-1)}\rho_{n,m-2_\alpha} + (2m_\alpha+1)\rho_{n,m} + \sqrt{(m_\alpha+2)(m_\alpha+1)}\rho_{n,m+2_\alpha} \right) \tilde{K}_{\alpha,\alpha}(\bar\zeta) \right] \\
& +\frac{1}{2\imath\hbar} \sum_{\alpha<\beta} a_\alpha a_\beta \left[\tilde{K}_{\alpha,\beta}(\bar\zeta)\left(\sqrt{(n_\alpha+1)(n_\beta+1)}\rho_{n+1_\alpha+1_\beta,m} + \sqrt{(n_\alpha+1)n_\beta}\rho_{n+1_\alpha-1_\beta,m} \right. \right. \\
& \left. + \sqrt{n_\alpha(n_\beta+1)}\rho_{n-1_\alpha+1_\beta,m} + \sqrt{n_\alpha n_\beta}\rho_{n-1_\alpha-1_\beta,m} \right) - \left(\sqrt{m_\alpha m_\beta}\rho_{n,m-1_\alpha-1_\beta} \right. \\
& + \sqrt{m_\alpha(m_\beta+1)}\rho_{n,m-1_\alpha+1_\beta} \\
& \left. \left. + \sqrt{(m_\alpha+1)m_\beta}\rho_{n,m+1_\alpha-1_\beta} + \sqrt{(m_\alpha+1)(m_\beta+1)}\rho_{n,m+1_\alpha+1_\beta} \right) \tilde{K}_{\alpha,\beta}(\bar\zeta) \right] ,
\end{aligned}
\tag{31}
$$

where $\Delta\tilde{F}_\alpha(\bar\zeta) = \tilde{F}_\alpha(\bar\zeta) - \sum_\beta U^*_{\alpha,\beta}\bar{F}_\beta$ is the operator that gives the quantum fluctuation of the force field along the quantized mode α. Note that in Eq. 31 some matrix elements of ρ must be set to zero to be consistent with Eq. 23.

The fifth term of Eq. 31 mixes quantum fluctuations along different quantized modes. This term is obviously absent when there is just one ionic DOF (compare with Eq. 26 of Ref. 23).

In numerical simulations, Eq. 31 and Eq. 9 are integrated iteratively[37] and consistently with the expansion of the average forces given in Eq. 27.

As a consequence of the CEID approximation, Eq. 23, the operator averages are obtained as

$$
\bar{O} = \sum_{|n|,|m|=0}^{N_{ceid}} \mathrm{Tr}_e \left\{ \rho_{n,m} O_{m,n} \right\} + \bar{O}^{(corr)}(N_{ceid}) ,
\tag{32}
$$

where the correction $|\bar{O}^{(corr)}(N_{ceid})| \to 0$ as $N_{ceid} \to \infty$. In practice, this correction can be evaluated numerically at run-time,[23] and it is small for converged CEID simulations (see Sec. V A).

III. INITIAL CONDITIONS AND IONIC GROUND-STATE

In this Section we derive variational estimates of the dimensional parameters a_α introduced in Sec. II C. In the limit $N_{ceid} \to \infty$ the choice of the values of these parameters becomes irrelevant, as the ionic basis set reaches completeness (see Sec. II D). The error made by representing an ionic wave function by a linear combination of a finite number of basis functions can be minimized by adjusting the values of the dimensional parameters. For instance, one can set a_α to match the spreading of the ionic wave function along the direction of the quantized mode α, as explained below.

Within the BO approximation[31], the ground-state density matrix of the total Hamiltonian, Eq. 1, takes the product form

$$\rho(t=0) = |0\rangle\langle 0| \otimes |\Phi_0(\bar{R}_0)\rangle\langle\Phi_0(\bar{R}_0)| \, , \tag{33}$$

where $\bar{R}_0$ is the classical equilibrium configuration of the ions, $\Phi_0(r; \bar{R}_0)$ the many-body adiabatic electronic ground-state (see Eq. 2) and $\Theta_0(R) = \langle R|0\rangle$ the BO ionic ground-state. Due to the large differences between electronic and ionic masses, the BO approximation usually gives a very good estimate of the total ground-state energy. Moreover, starting from a factorized (i.e., uncorrelated) initial condition, simplifies the study of the electron-ion correlation built up by the subsequent nonadiabatic evolution (see Sec. V).

According to Eq. 4, H_{bo}^0 is the BO Hamiltonian of the ions evolving on the electronic ground-state PES. By means of standard perturbation theory, this PES can be expanded up to the second order in $\Delta R = R - \bar{R}$ as

$$E_0(R) \simeq E_0(\bar{R}) - \sum_\alpha F_\alpha^{0,0}(\bar{R})\Delta R_\alpha + \frac{1}{2}\sum_{\alpha,\beta}\left(K_{\alpha,\beta}^{0,0}(\bar{R}) - 2\sum_{n>0}\frac{F_\alpha^{0,n}(\bar{R})F_\beta^{n,0}(\bar{R})}{E_n(\bar{R}) - E_0(\bar{R})}\right)\Delta R_\alpha\Delta R_\beta \, , \tag{34}$$

where

$$F_\alpha^{i,j}(\bar{R}) = \langle\Phi_i(\bar{R})|F_\alpha(\bar{R})|\Phi_j(\bar{R})\rangle \, , \tag{35}$$

$$K_{\alpha,\beta}^{i,j}(\bar{R}) = \langle\Phi_i(\bar{R})|K_{\alpha,\beta}(\bar{R})|\Phi_j(\bar{R})\rangle \tag{36}$$

and $\{\Phi_i(\bar{R})\}$ is the adiabatic electronic basis set for the classical ionic configuration $\bar{R}$ (see Eq. 2). In practice, the series defining the effective Hessian

$$\mathcal{K}_{\alpha,\beta}(\bar{R}) \stackrel{\text{def}}{=} K_{\alpha,\beta}^{0,0}(\bar{R}) - 2\sum_{n>0}\frac{F_\alpha^{0,n}(\bar{R})F_\beta^{n,0}(\bar{R})}{E_n(\bar{R}) - E_0(\bar{R})} \, , \tag{37}$$

13

must be truncated (See Sec. IV B).

By minimizing Eq. 34, one finds the classical equilibrium configuration, $\bar{R} = \bar{R}_0$. [We assume $\bar{R}_0$ is the global minimum.] The usual stationary conditions

$$F_\alpha^{0,0}(\bar{R}_0) = 0 \tag{38}$$

hold and the effective Hessian, $\mathcal{K}_{\alpha,\beta}(\bar{R}_0)$, is positive definite.

After the global minimum $\bar{R}_0$ has been found self-consistently—the adiabatic states depend parametrically on $\bar{R}$—the ground-state (many-body) electronic density matrix can be computed as

$$\rho_e(t = 0) = |\Phi_0(\bar{R}_0)\rangle\langle\Phi_0(\bar{R}_0)| . \tag{39}$$

A reasonable variational guess of the ionic ground-state is

$$\Theta_0(a; \Delta R) = \left[\prod_\alpha \left(\frac{1}{\pi a_\alpha^2}\right)^{\frac{1}{4}}\right] e^{-\frac{1}{2}\sum_{\alpha,\beta} D_{\alpha,\beta}\Delta R_\alpha \Delta R_\beta} , \tag{40}$$

where now $\Delta R = R - \bar{R}_0$ and the correlation matrix of quantized modes reads

$$D_{\alpha,\beta} = \sum_\gamma U_{\alpha,\gamma}\frac{1}{a_\gamma^2}U_{\gamma,\beta}^* . \tag{41}$$

Then, to find the best variational estimates of the dimensional parameters, one has to minimize the variational BO energy

$$E_{gs}\left[\Theta_0(a; \Delta R)\right] = \langle\Theta_0(a; \Delta R)| \sum_\alpha \frac{\hat{P}_\alpha^2}{2M_\alpha} + \frac{1}{2}\sum_{\alpha,\beta}\mathcal{K}_{\alpha,\beta}(\bar{R}_0)\Delta\hat{R}_\alpha\Delta\hat{R}_\beta|\Theta(a; \Delta R)\rangle \tag{42}$$

with respect to a.

Before minimizing Eq. 42, we note that Eq. 40 represents a proper bosonic wave function if and only if $D_{\alpha,\beta}$ is invariant with respect to permutations of equal atoms. This condition is automatically fulfilled if $U_{\alpha,\beta}$ is the unitary transform which diagonalizes the effective Hessian $\mathcal{K}_{\alpha,\beta}(\bar{R}_0)$. We shall refer to this set of quantized modes as the normal quantized modes.

If $U_{\alpha,\beta} = \mathbb{1}$, i.e., if Cartesian quantized modes are used, the a_α have to be the same for equal atoms. For instance, if all the atoms are equal,

$$a_\alpha = a \quad \forall \, \alpha . \tag{43}$$

14

In the following, we shall consider just these two sets of quantized modes.

When normal quantized modes are employed, Eq. 40 gives the exact solution of the quadratic BO problem (see Eq. 34) if

$$a_\alpha = \sqrt{\frac{\hbar}{M_0 \omega_\alpha}} \,, \tag{44}$$

where ω_α are the normal (angular) frequencies of the system. Note that, if the operators F_α and $K_{\alpha,\beta}$ are directly evaluated in real space, a computationally costly coordinate transform is required to compute the $\tilde{F}_\alpha$ and $\tilde{K}_{\alpha,\beta}$ appearing in Eq. 31 (see Eq. 25 and Eq. 26).

When Cartesian quantized modes are employed, Eq. 42 is minimized by

$$a = \sqrt{\frac{\hbar}{M_0 \tilde{\omega}}} \,, \tag{45}$$

where

$$\tilde{\omega} = \sqrt{\frac{1}{M_0} \frac{\sum_\alpha \mathcal{K}_{\alpha\alpha}(\bar{R}_0)}{D N_I}} \,. \tag{46}$$

In Sec. V A, we discuss how the convergence of a CEID simulation depends on the quantization scheme by comparing simulations in either normal or Cartesian quantized modes.

After the ionic ground-state or vacuum, $\Theta_0(R)$, is known, one can associate a formal meaning to the many-body ionic states, Eq. 20. Then, Eq. 33, can be formally interpreted as

$$\rho_{n,m}(t=0) = \begin{cases} \rho_e(t=0) & \text{if} \quad |n| = |m| = 0 \\ 0 & \text{otherwise} \end{cases} \,. \tag{47}$$

which provides—along with $\bar{P} = 0$ and $\bar{R} = \bar{R}_0$—the equilibrium BO initial conditions we use in numerical simulations (see Sec. V).

IV. REPRESENTATION OF THE ELECTRONIC STATES

In the previous Section we stated the extended CEID EOMs, Eq. 31, for the matrix elements $\rho_{n,m}$ which are but operators acting on the many-body electronic states (see Sec. II E). In this Section we discuss a consistent way to include electronic structure calculations within an extended CEID algorithm which is suitable for numerical applications.

A.   Physical constraints on the reduced electronic density matrix

A reduced electronic density matrix, $\rho_e^{(1)}$, which is obtained by tracing out all the electronic DOFs from the many-body electronic density matrix, ρ_e, represents a pure electronic state if it is idempotent:[38] $\rho_e^{(1)}\rho_e^{(1)} = \rho_e^{(1)}$. Such a pure electronic state is obtained, e.g., by using the *Aufbau principle* to build a Slater Determinant (SD) by filling up single particle levels.[31]

Due to the electron-ion interaction, the eigenvalues (natural populations) of $\rho_e^{(1)}$ can change and one must also consider reduced electronic density matrices which satisfy the weaker condition: $\mathrm{Tr}\{\rho_e^{(1)}\rho_e^{(1)}\} \leq \mathrm{Tr}\{\rho_e^{(1)}\}$. Since constraining all the reduced density matrices which satisfy this weaker condition is a hard task—known as the N-representability problem[38]—we decided so far to work directly with the many-body density matrix, i.e., in the space of the many-body electronic states. The integration of alternative electronic structure methods within a CEID algorithm is the subject of ongoing research.

B.   Interaction picture and evolving molecular orbitals

In the following, we assume $H_e(\bar{R}) = H_e^{(1)}(\bar{R}) + V(\bar{R})$, where

$$H_e^{(1)}(\bar{R}) = \sum_{i,j} H_{i,j}^{(1)}(\bar{R})c_i^\dagger c_j \ , \tag{48}$$

is a quadratic approximation of the many-body electronic Hamiltonian, H_e, and $c_i^\dagger(c_i)$ is the creation(annihilation) operator relative to the molecular orbital (MO) ϕ_i.[35] For instance, Eq. 48 can be the result of a Hartree-Fock (HF) calculation and $\{\phi_i\}$ the canonical HF orbitals.[31] In Sec. V we investigate in detail the much simpler case of a quadratic electronic Hamiltonian, $H_e = H_e^{(1)}$.

From the computational point of view, it is convenient to use an interaction picture representation of the electronic operators[35] to integrate out the quadratic part of the dynamics. This representation can be enforced by using a set of (orthonormalized) evolving molecular orbitals (EMOs) which satisfy:

$$\imath\hbar\frac{\partial \phi_i}{\partial t} = \sum_{j} H_{i,j}^{(1)}(\bar{R})\phi_j \ . \tag{49}$$

As usual, the time evolution obtained by integrating Eq. 49 defines a unitary transform of

the space spanned by the MOs. In practice, just a finite number of MOs can be included in a numerical simulation and an approximate unitary evolution is used.[39]

The set of all the SDs that are built starting from $M \geq N_e/2$ MOs provides a basis set for the (spin restricted) many-body electronic states of a system of N_e electrons.[31] This basis set is not complete, because just a finite number of MOs has been included. Nevertheless, it grows rapidly with M and N_e, its dimension being $\binom{2M}{N_e}$ (or $\binom{M}{N_e/2}[\binom{M}{N_e/2} + 1]/2$, if only SDs with $\bar{S}_z = 0$ are employed.)

The action of a unitary transform of the (finite) MO set defines a unitary transform of the subspace spanned by this many-body basis set. However, if only a subset of all the SDs built from a finite MO set is used, the action of a unitary transform on the MOs produces a transform of the subspace spanned by those SDs which is, in general, not invertible and so, not unitary. This non-unitary many-body evolution causes a systematic error in numerical simulation.

Finally, one can prove that the extended CEID EOMs in the interaction picture differ from Eq. 31 just in the Ehrenfest-like term (the second on the R.H.S.) which must be changed as follows:

$$+\frac{1}{\imath\hbar} \left[H_e(\bar{\zeta}), \rho_{n,m} \right] \rightarrow +\frac{1}{\imath\hbar} \left[V(\bar{\zeta}), \rho_{n,m} \right] \ . \tag{50}$$

This term is zero for a quadratic electronic Hamiltonian.

V. ELECTRON-ION COHERENCE STUDIED BY CEID

In this Section we demonstrate the capabilities of the extended CEID algorithm by studying the electron-ion analog of Rabi oscillations in a non-trivial model system. To this end, we use an artificial re-parametrization of the SSH Hamiltonian

$$H_{ssh} = \frac{1}{2} \sum_i \hat{P}_i^2 - \sum_{\langle i,j \rangle} \left(1 - \alpha |\hat{R}_i - \hat{R}_j| \right) (c_i^\dagger c_j + c_j^\dagger c_i) + \frac{1}{2} \sum_{\langle i,j \rangle} (\hat{R}_i - \hat{R}_j)^2 \ , \tag{51}$$

where $\langle i,j \rangle$ indicates nearest neighbor sites, $c_i^\dagger(c_i)$ creates(annihilates) an electron at site i, and α is the electron-ion coupling constant. [Adapted atomic units (a.u.) are used throughout this section.]

Although quadratic with respect to the electronic DOFs, H_{ssh} has a non-trivial spectrum including topological electron-ion excitations.[5] Therefore, the SSH model provides an

ideal test case to investigate the capability of the extended CEID algorithm to describe the electron-ion correlation. In particular, we wish to quantify the amount of electron-ion correlation which is missed if the quantum fluctuations of the ions are not considered.[8,15,16]
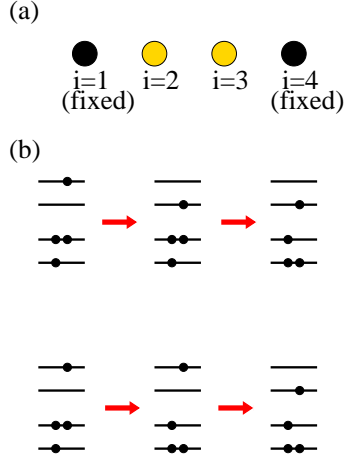

FIG. 1. (Color online) Panel (a): Sketch of the model SSH chain. Panel (b): Schematic representation of the two resonant nonradiative decay paths from the HOMO-1 → LUMO+1 state (left) to the HOMO → LUMO state (right).

Here we focus on an SSH chain made by four atoms (see Fig. 1(a)) with the two end atoms kept fixed (the fixed chain length is 60 a.u.). In this case, the exact electronic structure (frozen ions) can be calculated using 4 MOs and 21 SDs (Sec. IV B).

The chain is initially relaxed in the BO equilibrium configuration (Sec. III) and then vertically excited (i.e., without changing ρ_I) by promoting an electron from the HOMO-1 to the LUMO+1, i.e., the HOMO-1 → LUMO+1 (many-body) state is initially excited.

By diagonalizing separately the electronic and ionic parts of Eq. 51 in the $\alpha = 0$ case, i.e., no electron-ion interaction, one finds that the energy gap between the HOMO-1 → LUMO+1 and the HOMO → LUMO+1 (or HOMO-1 → LUMO) states is equal to the quantum of vibration of the lowest normal mode of the chain. Owing to particle-hole symmetry, the energy gap between the HOMO → LUMO+1 (or HOMO-1 → LUMO) and the HOMO → LUMO states is also equal to the same quantum of vibration.

These resonances between single particle electronic transitions and quantized vibrations of the chain yield some accidental degeneration in the electron-ion energy spectrum, e.g., the electronic HOMO-1 → LUMO+1 state is degenerate to the HOMO → LUMO state *plus*

18

a double excitation of the lowest quantized mode of the chain. As a consequence, although the electronic states HOMO-1 $\to$ LUMO+1 and HOMO $\to$ LUMO are not degenerate, it is possible to have a resonant nonradiative transition from the HOMO-1 $\to$ LUMO+1 state to the HOMO $\to$ LUMO state (through the intermediate HOMO $\to$ LUMO+1 or HOMO-1 $\to$ LUMO states) by the spontaneous emission of two quantized excitations of the chain, as depicted in Fig. 1(b).

In the $\alpha > 0$ case, the accidental electron-ion degeneracies are lifted and, in analogy with the theory of Rabi oscillations,[25,32] for small values of α one expects to observe periodic transitions among the almost degenerate electron-ion many-body states.

To investigate quantum coherence in the electron-ion analog of Rabi oscillations, one can expand the formal solution of the total quantum Liouville equation

$$\frac{\partial \rho(t)}{\partial t} = \frac{1}{\imath \hbar}[H_{ssh}, \rho(t)] \,, \tag{52}$$

by means of the Schmidt decomposition[40] as

$$\rho(t) = \sum_i P_i(t)|\Theta_I^{(i)}(t)\rangle\langle\Theta_I^{(i)}(t)| \otimes |\Phi_e^{(i)}(t)\rangle\langle\Phi_e^{(i)}(t)| \,, \tag{53}$$

where $|\Theta_I^{(i)}(t)\rangle$ represents the ionic and $|\Phi_e^{(i)}(t)\rangle$ the electronic states. In general $|\Phi_e^{(i)}(t)\rangle$ are different from the adiabatic states. In particular, even if Eq. 53 is initially factorized as in Eq. 33, it might not be factorizable during the subsequent (nonadiabatic) quantum dynamics. When not globally, i.e., at all times, factorizable, Eq. 53 describes quantum coherence (linear superposition) among factorized electron-ion evolutions. Since ED is based on a factorized density matrix (see Eq. 10), electron-ion correlations due to quantum coherence are not accounted for by an ED simulation.

Through Eq. 53, one can define the Frobenius norm of $\rho(t)$ as

$$F_e(t) \stackrel{\text{def}}{=} \sqrt{\sum_i P_i^2(t)} \,, \tag{54}$$

and see that factorizable solutions have $F_e(t) = 1$, while nonfactorizable solutions have $F_e(t) < 1$. [We assume that all the states in Eq. 53 are properly orthonormalized.] In particular, $F_e(t) = 1$ for an ED simulation.

Numerical solutions of Eq. 52 by the extended CEID algorithm presented in this article are shown in the next Sections.

A. Convergence with respect to the quantum fluctuations of the ions
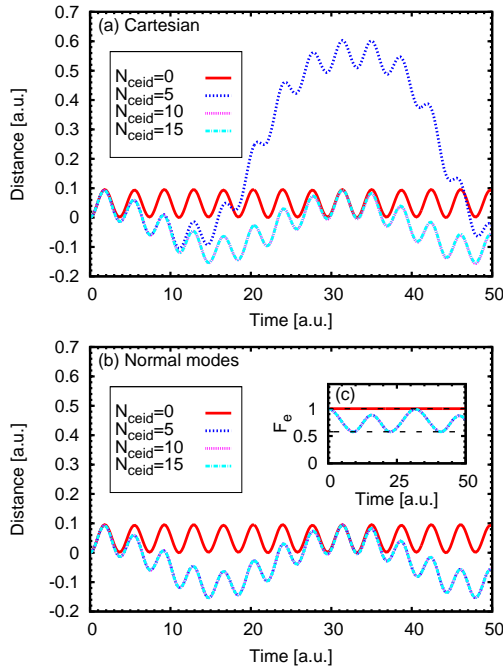

FIG. 2. (Color online) Convergence with respect to N_{ceid}: All simulations with $N_{coor} = 2$, and $\alpha = 0.2$. Panel (a): Time evolution of the variation of $\bar{R}_3 - \bar{R}_2$ for different N_{ceid} using Cartesian quantized modes. Panel (b): Same as panel (a), but using normal quantized modes. Inset (c): Time evolution of Frobenius norm, F_e, same simulations as in panel (b). The theoretical lower limit for a three-level system, $F_e = 1/\sqrt{3}$, is indicated.

In Fig. 2 we plot the time evolutions of the variation (with respect to the initial conditions) of the average distance, $\bar{R}_3 - \bar{R}_2$, between the two central atoms of the chain (see Fig. 1(a)). Results in panel (a) have been obtained by an expansion of the quantum fluctuations of the ions relative to Cartesian quantized modes, while normal quantized modes have been used for the results in panel (b) (see Sec. III). In both panels, results from $N_{ceid} = 0, 5, 10, 15$ dynamics (see Sec. II F) are reported. A complete many-body basis set and EMOs (see Sec. IV B) have been used.

The initial chain BO geometry, $\bar{R}_0$ (see Sec. III), or Frank-Condon geometry, differs from the equilibrium geometry on the HOMO-1 $\rightarrow$ LUMO+1 PES, $\bar{R}_0'$, because of the electron-ion interaction. As a consequence, all time evolutions show fast adiabatic oscillations about

20

$\bar{R}_0'$. The angular frequency, ω_{adia}, of these adiabatic oscillations is very close to $\sqrt{3}$ a.u., i.e., they all correspond to the highest normal mode of the system (see Sec. V B). In particular, the $N_{ceid} = 0$ time evolutions, for both Cartesian and normal quantized modes, only show these fast adiabatic oscillations.

With both Cartesian and normal quantization, the systematic inclusion of quantum fluctuations of the ions—by increasing N_{ceid}— eventually leads to a well-converged time evolution of the variation of $\bar{R}_3 - \bar{R}_2$. In fact, $N_{ceid} = 10$ and $N_{ceid} = 15$ evolutions are already indistinguishable in both Fig. 2(a) and Fig. 2(b). [4356 and 18496 matrix elements $\rho_{n,m}$ are propagated according to Eq. 31 in the $N_{ceid} = 10$ and $N_{ceid} = 15$ cases, respectively (see Appendix B).] Manifestly, when convergence is reached, the choice of the quantized modes becomes immaterial. However, it is clear from the comparison of the two panels of Fig. 2 that convergence is more regular if normal quantized modes are employed.

Converged time evolutions display fast adiabatic oscillations as in the $N_{ceid} = 0$ case, but modulated by a slower periodic motion. These slow oscillations are the signature of an electronic transition from the initial HOMO-1 $\to$ LUMO+1 excited state to a lower one (see Fig. 1(b)). This transition must be due to a coherent quantum process, because the Frobenius norm, F_e, (see Sec. V) also shows oscillations for $N_{ceid} > 0$ (see Fig. 2(c)). These F_e oscillations are bounded by 1—the ED limit—and $1/\sqrt{3}$—the theoretical limit for a maximally entangled[40] three-level system (see Fig. 1(b)). In addition, $F_e(t)$ can be decomposed as the sum of two harmonic oscillations of angular frequency ω_{rabi} and $2\omega_{rabi}$, respectively, where ω_{rabi} is the angular frequency of the slow $\bar{R}_3 - \bar{R}_2$ oscillations.

The dynamics of the electronic transitions responsible of the slow $\bar{R}_3 - \bar{R}_2$ oscillations can be deduced from Fig. 3(a), where the populations of the many-body excited states depicted in Fig. 1(b) are reported. [Note that those states are built using a set of EMOs (see Sec. IV B).] In the case of an $N_{ceid} = 0$ simulation (not shown), the HOMO-1 $\to$ LUMO+1 state is the only electronic state populated.

Finally, in Fig. 3(b) we plot converged time evolutions of the variation of $\bar{R}_3 - \bar{R}_2$ with quantum fluctuations of the ions along only one ($N_{coor} = 1$, see Sec. II C) of the two normal quantized modes and the results of Fig. 2(b) as a reference. If quantum fluctuations of the ions are permitted just along the highest, nonresonant (see Sec. V and Fig. 1), normal quantized mode, only fast adiabatic oscillations are observed. On the other hand, a time evolution with quantum fluctuations along this mode suppressed is not distinguishable from
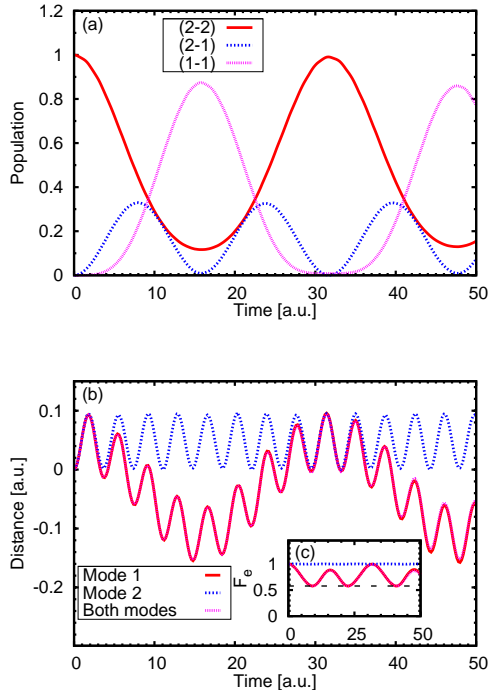
21

FIG. 3. (Color online) Selecting quantum fluctuations of the ions: All simulations with $N_{ceid} = 10$, and $\alpha = 0.2$. Panel (a): Time evolution of the electronic population of the HOMO-1 $\rightarrow$ LUMO+1 (2-2), a symmetric combination of HOMO-1 $\rightarrow$ LUMO and HOMO $\rightarrow$ LUMO+1 (2-1), and HOMO $\rightarrow$ LUMO (1-1) states, with quantum fluctuations of the ions along both modes. Panel (b): Time evolution of the variation of $\bar{R}_3 - \bar{R}_2$ with quantum fluctuations of the ions along one—either the lowest (mode 1) or the highest (mode 2)—or both (initial) normal modes of the chain. [The first and third evolutions are superimposed at the scale of this figure.] Inset (c): Time-evolution of Frobenius norm, F_e, same simulations as in panel (b). The theoretical lower limit for a three-level system, $F_e = 1/\sqrt{3}$, is indicated.

a reference evolution with quantum fluctuations of the ions permitted along both quantized modes. In addition, an $N_{ceid} = 10$ time evolution with only quantum fluctuations relative to the non-resonant quantization mode shows trivial Frobenius norm evolution, $F_e(t) = 1$, like the $N_{ceid} = 0$ case (see Fig. 3(c)).

Results of this Section clearly suggest that, if symmetry adapted, e.g., normal, quantized modes are employed, one can just include the quantum fluctuations of the ions along the resonant quantized modes without compromising the quality of a CEID simulation. When

22

possible, selection of the quantized modes gives a very effective way to decrease the computational cost of the extended CEID algorithm (see Appendix B).

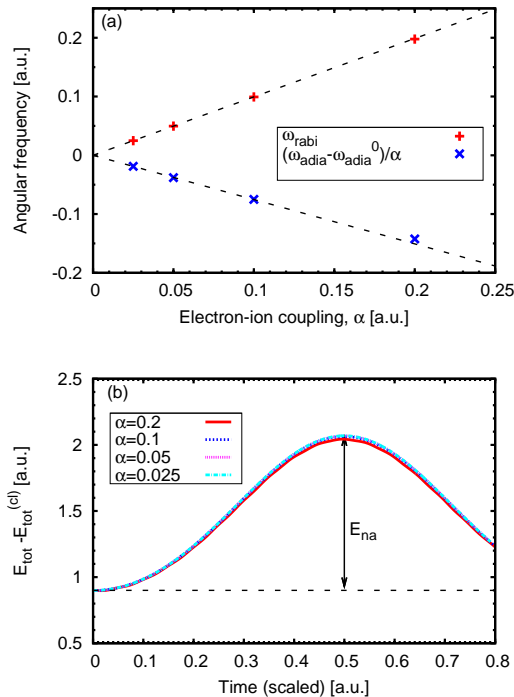## B. Analog of Rabi oscillations in a coupled electron-ion system

FIG. 4. (Color online) Coherent energy transfer between electrons and ions: All simulations with $N_{coor} = 2$, $N_{ceid} = 10$. Panel (a): Rabi (ω_{rabi}) and adiabatic (ω_{adia}) angular frequencies as a function of the electron-ion coupling constant, α. [$\omega_{adia}^0 = \sqrt{3}$ a.u.] Panel (b): Scaled time evolution of the difference between the total and classical (total) energies, Eq. 55, for different electron-ion coupling constant, α. [Some evolutions are superimposed at the scale of this figure.]

In Fig. 4(a) we show ω_{rabi} and ω_{adia} as functions of α. Their values have been obtained by fitting the corresponding time evolutions of the variation of $\bar{R}_3 - \bar{R}_2$ by the function $f(t) = f_0 - c_1 \cos(\omega_{adia}t) + c_2 \cos(\omega_{rabi}t) - c_3 \cos(2\omega_{rabi}t)$. The angular frequency ω_{rabi} scales linearly with α, strongly suggesting that the slow oscillations of the variation of $\bar{R}_3 - \bar{R}_2$ are caused by a coherent quantum electron-ion dynamics analog to the Rabi oscillations.[32] In addition, the linear fitting of $(\omega_{adia} - \omega_{adia}^0)/\alpha$, with $\omega_{adia}^0 = \sqrt{3}$, in Fig. 4(a) confirms

that the fast oscillations are linked to the highest normal mode of the system (see Sec. V A). [The quadratic correction in α is due to the corrections to the bare Hessian, see Eq. 37.]

Finally, in Fig. 4(b) we plot the time evolution of the difference between the total energy, $E_{tot} = \text{Tr}\{\rho H\}$, and the classical (total) energy,

$$E_{tot}^{(cl)} = \sum_{\alpha=1}^{N_I} \frac{\bar{P}_\alpha^2}{2M_\alpha} + \text{Tr}\{\rho H_e(\bar{R})\} \, , \qquad (55)$$

for several values of electron-ion coupling constant, α. [Time scales have been rescaled by $2\pi/\omega_{rabi}(\alpha)$.] This energy difference can be qualitatively assigned to the quantum DOFs of the ions. Indeed, this is exactly zero in ED (compare Eq. 55 with Eq. 14).

In the converged $N_{ceid} = 10$ cases shown in Fig. 4(b), $E_{tot} - E_{tot}^{(cl)}$ starts from a finite value due to the zero-point quantum fluctuations of the ions (see Sec. II D) and subsequently increases as the population of the initial HOMO-1 $\rightarrow$ LUMO+1 state decreases, and vice versa (see Fig. 3(a)).

We indicate with E_{na} the difference between the initial and maximum values of $E_{tot} - E_{tot}^{(cl)}$ (see Fig. 4(b)). E_{na} can be viewed as the amount of energy that must be provided to the quantum DOFs of the ions in order for the system to decay nonadiabatically from the initial HOMO-1 $\rightarrow$ LUMO+1 state (see Fig. 3(a) and Fig. 1(b)). Note that E_{na} does not depend on α, although the magnitude of the electron-ion coupling constant determines the rate of this nonadiabatic decay, and the subsequent inverse process. [The system is closed, so energy is always reversibly exchanged.]

VI.   DISCUSSION AND CONCLUSIONS

Numerical results reported in Sec. V clearly demonstrate that quantum coherence between electron and ion dynamics can be accurately simulated by the extended CEID algorithm presented in this article. In particular, we have shown that, when quantum coherence is properly accounted for, the analog of Rabi oscillations among several (e.g., three) resonating electron-ion states can be observed in the evolution of a model system (e.g., a 4-atom SSH chain).

We have also illustrated some important computational features of the extended CEID algorithm, namely: 1) Systematic convergence by increasing N_{ceid}, i.e., the parameter which controls the amount of quantum fluctuations of the ions included in the simulation. 2)

24

The possibility of including selectively—according to the dynamical symmetries—quantum fluctuations along those ionic collective modes which are more strongly coupled with electronic transitions, i.e., the active ionic modes. 3) Compatibility with electronic structure calculations based on many-body electronic states, e.g., Hartree-Fock and post-Hartree-Fock methods of Quantum Chemistry.

A 4-atom SSH chain provided a suitable model to test the extended CEID capabilities. In this Section, we briefly discuss the applicability of the extended CEID algorithm to more physically relevant models. First of all, one can start by considering longer SSH chains, since they have been often used to model single-stranded π-conjugated polymers.[6] The extended CEID algorithm can be still applied to model the time evolution of chains up to a few tens of atoms for a few hundreds of femtoseconds, although with quantum fluctuations of the ions allowed only along a very restricted set of collective atomic modes, e.g., the highest optical vibrations.[30]

The computational cost of the extended CEID algorithm scales polynomially with respect to the number of active ionic modes, N_{coor} (see Appendix B). The scaling of extended CEID algorithm has to be contrasted to the bare exponential scaling of the exact numerical solution of the time-dependent Schrödinger equation.[23] Besides, the computational cost of the extended CEID algorithm can be greatly reduced by selecting a minimal set of active modes. These active quantized modes can be chosen by estimating their coupling with the electronic transitions (the nonadiabatic coupling[11]) without altering the quality of the CEID simulation, as illustrated in Sec. V A.

The application of the extended CEID algorithm to semiempirical models of π-conjugated polymers including electron-electron correlation[4,41,42] is the subject of ongoing research, along with important algorithmic improvements (e.g., use of sparse linear algebra and code parallelization).

In conclusion, in this article we have extended the Correlated Electron-Ion Dynamics (CEID) algorithm introduced in Ref. 23 to simulate the quantum electron-ion evolution of a many-atom system. As in Ref. 23, the extended CEID algorithm systematically converges to the exact solution of the time-dependent Schrödinger equation. We have illustrated the capabilities of the extended CEID by studying a 4-atom SSH chain, reparametrized to enhance quantum coherence between the electron and ion dynamics. In particular, we have observed periodic transitions between three many-body electronic states accompanied by a

modification of the quantum state of the ions, i.e., the analog of the Rabi oscillations. No such oscillations have been observed when only zero-point quantum fluctuations of the ions about their Ehrenfest trajectory in phase space have been included in a CEID simulation. Convergence and computational cost of the extended CEID algorithm have been also discussed. Applications of the extended CEID algorithm to more realistic problems, e.g., the nonradiative relaxation of π-conjugated polymers, are the subject of ongoing research and future publications.[30]

Appendix A: Time-dependence of the quantum operators in a Lagrangian-like picture

In this Appendix we show a formal procedure to transform operators from the original Schrödinger picture to a kind of Heisenberg picture[32] analogous to the Lagrangian flow specification of fluid dynamics.[34]

Since $\hat{P}$ is the generator of the spatial translations[32], a generic ionic wave function $\Psi(R)$ is mapped into $e^{+\frac{1}{i\hbar}\bar{R}\hat{P}}\Psi(R)$ by translating the origin of the positions by $\bar{R}$. By means of the Fourier transform, one can also prove that $\Psi(R)$ is mapped into $e^{-\frac{1}{i\hbar}\bar{P}\hat{R}}\Psi(R)$ by translating the origin of the momenta by $\bar{P}$.

If $\bar{P}$ and $\bar{R}$ are time-dependent, the combined effect of a momentum translation by $\bar{P}$ and a position translation by $\bar{R}$ gives an implicitly time-dependent wave function, $e^{+\frac{1}{i\hbar}\bar{R}(t)\hat{P}-\frac{1}{i\hbar}\bar{P}(t)\hat{R}}\Psi(R)$. E.g., this is the case of the many-body ionic states defined in Eq. 20. Since this implicit time-dependence can be easily factorized out from the wave functions, one can transfer it to the operators, as it is done in the usual Heisenberg picture of quantum dynamics.[32] This way one ends with (implicitly) time-independent wave functions and (implicitly) time-dependent operators. [Both wave functions and operators can still have an

explicit time-dependence.]

Let $O = f(\hat{P}, \hat{R})$ be an operator in the original Schrödinger picture which is a function of the momentum and position operators, $\hat{P}$ and $\hat{R}$. Then we define the transformed operator in the Lagrangian-like picture as

$$O_L(\bar{P}, \bar{R}) \overset{\text{def}}{=} e^{-\frac{1}{\imath\hbar}\bar{R}\hat{P}+\frac{1}{\imath\hbar}\bar{P}\hat{R}} O e^{+\frac{1}{\imath\hbar}\bar{R}\hat{P}-\frac{1}{\imath\hbar}\bar{P}\hat{R}} . \tag{A1}$$

Thanks to the Baker-Campbell-Hausdorff theorem,[32] we have that

$$
\begin{aligned}
& e^{-\frac{1}{\imath\hbar}\bar{R}\hat{P}+\frac{1}{\imath\hbar}\bar{P}\hat{R}} O e^{+\frac{1}{\imath\hbar}\bar{R}\hat{P}-\frac{1}{\imath\hbar}\bar{P}\hat{R}} \\
= & e^{+\frac{1}{\imath\hbar}\bar{P}\hat{R}} e^{-\frac{1}{\imath\hbar}\bar{R}\hat{P}} O e^{+\frac{1}{\imath\hbar}\bar{R}\hat{P}} e^{-\frac{1}{\imath\hbar}\bar{P}\hat{R}} \\
= & e^{-\frac{1}{\imath\hbar}\bar{R}\hat{P}} e^{+\frac{1}{\imath\hbar}\bar{P}\hat{R}} O e^{-\frac{1}{\imath\hbar}\bar{P}\hat{R}} e^{+\frac{1}{\imath\hbar}\bar{R}\hat{P}} ,
\end{aligned}
\tag{A2}
$$

and so the operator transform (or superoperator) defined in Eq. A1 can be seen as the composition of two superoperators which commute. Therefore, the dependence of O_L on $\bar{P}$ and $\bar{R}$ is classical because the transform in Eq. A1 does not depend on the order of the terms.

By applying Eq. A1 to the momentum and position operators, one finds that (see Eq. 16)

$$\hat{P}_L = \hat{P} + \bar{P}\mathbb{1} \Rightarrow \hat{P} = (\Delta\hat{P})_L . \tag{A3a}$$

$$\hat{R}_L = \hat{R} + \bar{R}\mathbb{1} \Rightarrow \hat{R} = (\Delta\hat{R})_L , \tag{A3b}$$

Hence, for $O = f(\hat{P}, \hat{R})$, one also finds that

$$
\begin{aligned}
O_L = & f(\hat{P} + \bar{P}\mathbb{1}, \hat{R} + \bar{R}\mathbb{1}) \simeq f(\bar{P}, \bar{R})\mathbb{1} \\
& + \frac{\partial f}{\partial P}(\bar{P}, \bar{R})(\Delta\hat{P})_L + \frac{\partial f}{\partial R}(\bar{P}, \bar{R})(\Delta\hat{R})_L \\
& + \cdots
\end{aligned}
\tag{A4}
$$

which confirms that in the Lagrangian-like picture the operators are just translated by $\bar{P}$ and $\bar{R}$ with respect to the original operators in the Schrödinger picture (see Eq. 17).

By means of Eq. A2 and Eq. A3, the partial derivatives of any O_L with respect to $\bar{P}$ and $\bar{R}$ can be uniquely defined as

$$\frac{\partial O_L}{\partial \bar{P}} = \frac{1}{\imath\hbar}[(\Delta\hat{R})_L, O_L] , \tag{A5a}$$

$$\frac{\partial O_L}{\partial \bar{R}} = \frac{1}{\imath\hbar}[O_L, (\Delta\hat{P})_L] . \tag{A5b}$$

27

Therefore, by means of Eq. 13 and Eq. A5, one derives—in analogy with the definition of the total or material derivative in fluid dynamics[34]—that

$$
\begin{aligned}
\frac{\mathrm{d}\rho_L}{\mathrm{d}t} &= \frac{\partial \rho_L}{\partial t} + \frac{\partial \rho_L}{\partial \bar{P}}\dot{P} + \frac{\partial \rho_L}{\partial \bar{R}}\dot{R} \\
&= \frac{1}{\imath\hbar}[H_L + \dot{P}(\Delta\hat{R})_L - \dot{R}(\Delta\hat{P})_L, \rho_L] \\
&\stackrel{\mathrm{def}}{=} \frac{1}{\imath\hbar}[H_L^{(mat)}, \rho_L] \; .
\end{aligned}
\tag{A6}
$$

Eq. A6 agrees with a similar expression obtained in the Appendix B of Ref. 23 by employing the Wigner transform.

Finally, by means of Eq. A6 and Eq. A5, the following EOM for the operator averages is found:

$$
\frac{\mathrm{d}}{\mathrm{d}t}\mathrm{Tr}\{\rho O\} = \frac{\mathrm{d}}{\mathrm{d}t}\mathrm{Tr}\{\rho_L O_L\} = \mathrm{Tr}\left\{\rho_L \frac{\mathrm{d}O_L}{\mathrm{d}t}\right\} \; ,
\tag{A7}
$$

where

$$
\frac{\mathrm{d}O_L}{\mathrm{d}t} = \frac{1}{\imath\hbar}[O_L, H_L^{(mat)}] + \frac{\partial O_L}{\partial \bar{P}}\dot{P} + \frac{\partial O_L}{\partial \bar{R}}\dot{R}
\tag{A8}
$$

is the Heisenberg EOM for O_L in the Lagrangian-like picture.

For the sake of simplicity, in the body of the article we have always dropped the subscript L whenever the use of the Lagrangian-like picture was explicitly declared.

Appendix B: Scaling of the extended CEID algorithm

The linear dimension, D_I, of the approximate ionic Hilbert space, $\mathcal{S}_{N_{ceid}}$, defined in Sec. II D can be computed as follows: Consider the subset, $\mathcal{S}^{(n)}$, spanned by the ionic states $|i\rangle$ (see Sec. II C) so that $|i| = n$. Therefore, $\mathcal{S}_{N_{ceid}} = \bigcup_{n=0}^{N_{ceid}} \mathcal{S}^{(n)}$. As a consequence, by using standard combinatorics, one obtains that

$$
D_I = \sum_{i=0}^{N_{ceid}} \binom{i + N_{coor} - 1}{i} = \binom{N_{ceid} + N_{coor}}{N_{coor}} \; .
\tag{B1}
$$

Since the number of matrix elements $\rho_{n,m}$ included in Eq. 31 is equal to D_I^2, the computational cost of updating all non-zero $\rho_{n,m}$ at each time step will scale as

$$
D_I^2 \simeq
\begin{cases}
\frac{1}{2\pi N_{coor}}\left(\frac{N_{ceid}}{N_{coor}}\right)^{2N_{coor}} & N_{coor} \ll N_{ceid} \; . \\
\frac{1}{2\pi N_{ceid}}\left(\frac{N_{coor}}{N_{ceid}}\right)^{2N_{ceid}} & N_{ceid} \ll N_{coor} \; ,
\end{cases}
\tag{B2}
$$

28

The case $N_{coor} \ll N_{ceid}$ of Eq. B2, which also includes the limit $N_{ceid} \to \infty$, yields the bare exponential scaling with N_{coor} of the exact numerical solution of the time-dependent Schrödinger equation.[23] This limit is relevant for resonant electron-ion systems, e.g., the model considered in Sec. V, in which the quantum fluctuations of the ions are strongly enhanced by multiple, periodic electron-ion interactions. In this case the scaling with N_{coor} is exponential. However, since electron-ion resonances usually involve one or few ionic quantized modes, i.e., $N_{coor} \ll DN_I$, one can still converge the CEID evolution of model Hamiltonians for few tens of atoms.[30]

The case $N_{ceid} \ll N_{coor}$ of Eq. B2 yields a polynomial scaling with N_{coor}, although the degree of the polynomial, $2N_{ceid}$, can be large. This case can be relevant for nonresonant systems, e.g., thermalized systems at low temperature, in which: i) Quantum ionic effects cannot be neglected. ii) Quantized ionic modes are only slightly excited, i.e., N_{ceid} can be kept small. Therefore, also in this case, converged CEID simulations might be feasible.

REFERENCES

[1] F. Cacialli, Phil. Trans. R. Soc. Lond. A, **358**, 173 (2000); S. R. Forrest, Nature, **428**, 911 (2004).

[2] G. D. Scholes and G. Rumbles, Nature materials, **5**, 683 (2006).

[3] H. Zhao, S. Mazumdar, C. X. Sheng, M. Tong, and Z. V. Vardeny, Phys. Rev. B, **73**, 075403 (2006).

[4] R. Pariser and R. Parr, J. Chem. Phys, **21**, 466 (1953); J. A. Pople, Trans. Faraday Soc., **49**, 1375 (1953).

[5] W. P. Su, J. R. Schrieffer, and A. J. Heeger, Phys. Rev. Lett., **42**, 1698 (1979); Phys. Rev. B, **22**, 2099 (1980); A. J. Heeger, Rev. Mod. Phys., **73**, 681 (2001).

[6] Z. An, C. Q. Wu, and X. Sun, Phys. Rev. Lett., **93**, 216407 (2004).

[7] A. Anderson, Phys. Rev. Lett., **74**, 621 (1995); J. Caro and L. L. Salcedo, Phys. Rev. A, **60**, 842 (1999); F. Agostini, S. Caprara, and G. Ciccotti, Europhys. Lett., **78**, 30001 (2007).

[8] J. le Page, D. R. Mason, and W. M. C. Foulkes, J. Phys.: Condens. Matter, **20**, 125212 (2008).

[9] E. J. Heller, J. Chem. Phys, **75**, 2923 (1981).

[10]J. C. Tully and R. K. Preston, J. Chem. Phys., **55**, 562 (1971); J. Tully, **93**, 1061 (1990).

[11]J. C. Tully, Faraday Discuss., **110**, 407 (1998); M. D. Hack and D. G. Truhlar, J. Phys. Chem. A, **104**, 7917 (2000).

[12]R. Kapral and G. Ciccotti, J. Chem. Phys., **110**, 8919 (1999); S. Nielsen, R. Kapral, and G. Ciccotti, **115**, 5805 (2001); D. Mac Kernan, G. Ciccotti, and R. Kapral, **116**, 2346 (2002).

[13]M. Ben-Nun, J. Quenneville, and T. J. Martinez, J. Phys. Chem. A, **104**, 5161 (2000); M. Ben-Nun and T. J. Martinez, Adv. Chem. Phys., **121**, 439 (2002).

[14]N. L. Doltsinis and D. Marx, Phys. Rev. Lett., **88**, 166402 (2002).

[15]A. P. Horsfield, D. R. Bowler, A. J. Fisher, T. N. Todorov, and C. G. Sánchez, J. Phys.: Condens. Matter, **16**, 8251 (2004); **17**, 4793 (2005); A. P. Horsfield, D. R. Bowler, H. Ness, C. G. Sánchez, T. N. Todorov, and A. J. Fisher, Rep. Prog. Phys., **69**, 1195 (2006).

[16]E. J. McEniry, Y. Wang, D. Dundas, T. N. Todorov, L. Stella, R. P. Miranda, A. J. Fisher, A. P. Horsfield, C. P. Race, D. R. Mason, W. M. C. Foulkes, and A. P. Sutton, Eur. Phys. J. B, **77**, 305 (2010).

[17]X. Li, J. C. Tully, H. B. Schlegel, and M. J. Frisch, J. Chem. Phys, **123**, 084106 (2005).

[18]E. Tapavicza, I. Tavernelli, and U. Rothlisberger, Phys. Rev. Lett., **98**, 023001 (2007).

[19]J. L. Alonso, X. Andrade, P. Echenique, F. Falceto, D. Prada-Gracia, and A. Rubio, Phys. Rev. Lett., **101**, 096403 (2008).

[20]As in Ref. 15, we denote by 'ion' a nucleus and its core electrons lumped together, even if the atom is not truly ionized. Hence, 'ionic' is used instead of 'nuclear' throughout the article.

[21]A. P. Horsfield, D. R. Bowler, A. J. Fisher, T. N. Todorov, and M. J. Montgomery, J. Phys.: Condens. Matter, **16**, 3609 (2004); A. P. Horsfield, D. R. Bowler, and A. J. Fisher, **16**, L65 (2004); D. R. Bowler, A. P. Horsfield, C. G. Sánchez, and T. N. Todorov, **17**, 3985 (2005); E. J. McEniry, D. R. Bowler, D. Dundas, A. P. Horsfield, C. G. Sánchez, and T. N. Todorov, **19**, 196201 (2007); E. J. McEniry, T. Frederiksen, T. N. Todorov, D. Dundas, and A. P. Horsfield, Phys. Rev. B, **78**, 035446 (2008); E. J. McEniry, T. N. Todorov, and D. Dundas, J. Phys.: Condens. Matter, **21**, 195304 (2009).

[22]T. J. Martinez, Acc. Chem. Res., **39**, 119 (2006); M. H. Kim, L. Shen, H. Tao, T. J. Martinez, and A. S. Suits, Science, **315**, 1561 (2007).

[23]L. Stella, M. Meister, A. J. Fisher, and A. P. Horsfield, J. Chem. Phys., **127**, 214104

(2007).

[24] Y. Wang, Phys. Rev. B, **79**, 235102 (2009).

[25] X. Q. Li, H. Nakayama, and Y. Arakawa, Phys. Rev. B, **59**, 5069 (1999); M. I. Vasilevskiy, R. P. Miranda, E. V. Anda, and S. S. Makler, Semicond. Sci. Technol., **19**, S312 (2004).

[26] G. S. Engel, T. R. Calhoun, E. L. Read, T. K. Ahn, T. Mančal, Y. C. Cheng, R. E. Blankenship, and G. R. Fleming, Nature, **446**, 782 (2007); H. Lee, Y. H. Cheng, and G. R. Fleming, Science, **316**, 1462 (2007).

[27] E. Collini and G. D. Scholes, Science, **323**, 369 (2009); E. Collini, C. Y. Wong, K. E. Wilk, P. M. G. Curmi, P. Brumer, and G. D. Scholes, Nature, **463**, 644 (2010).

[28] S. Jang, Y. C. Cheng, D. R. Reichman, and J. D. Eaves, J. Chem. Phys., **129**, 101104 (2008); A. Ishizaki and G. R. Fleming, J. Chem. Phys, **130**, 234110 (2009); **130**, 234111 (2009); Y. C. Cheng and G. R. Fleming, Annu. Rev. Phys. Chem., **60**, 241 (2009).

[29] H. Tamura, E. R. Bittner, and I. Burghardt, J. Chem. Phys., **126**, 021103 (2007); **127**, 034706 (2007); H. Tamura, J. G. S. Ramon, E. R. Bittner, and I. Burghardt, Phys. Rev. Lett., **100**, 107402 (2008); H. Tamura, J. Chem. Phys., **130**, 214705 (2009).

[30] L. Stella, R. P. Miranda, A. P. Horsfield, and A. J. Fisher, In preparation.

[31] C. J. Cramer, *Essential computational chemistry*, 2nd ed. (Wiley, 2004).

[32] J. J. Sakurai, *Modern Quantum Mechanics*, revised ed. (Addison Wesley, 1993).

[33] J. le Page, D. R. Mason, C. P. Race, and W. M. C. Foulkes, New J. Phys., **11**, 013004 (2009).

[34] A. L. Fetter and J. D. Walecka, *Theoretical Mechanics of Particles and continua* (Dover, 2004).

[35] A. L. Fetter and J. D. Walecka, *Quantum Theory of Many-Particle Systems* (Dover, 2003).

[36] Matrix elements $(F_\alpha)_{m,n}$ are obtained by expanding the operator F_α as in Eq. 17. To be consistent, H_e and F_α must be expanded up to the same order in $\Delta\hat{R}$.

[37] In the current implementation of the code we use the Verlet algorithm to integrate Eq. 9 and second order Runge-Kutta to integrate Eq. 31.

[38] U. Fano, Rev. Mod. Phys., **29**, 74 (1957); R. McWeeny, **32**, 335 (1960); A. J. Coleman, **35**, 668 (1963).

[39] For the model systems investigated in Sec. V, exact numerical integration of Eq. 49 by computing the exponential of $H^{(1)}$ at each time step is feasible.

[40] M. A. Nielsen and I. L. Chuang, *Quantum Computation and Quantum Information* (Cam-

bridge University Press, 2000).

[41] Z. G. Soos, S. Ramasesha, D. S. Galvão, R. G. Kepler, and S. Etemad, Synt. Met., **54**, 35 (1993); W. Barford, R. J. Bursill, and R. W. Smith, Phys. Rev. B, **66**, 115205 (2002); B. Di, Z. An, Y. C. Li, and C. Q. Wu, Eurohys. Lett., **79**, 17002 (2007).

[42] R. P. Miranda, A. J. Fisher, L. Stella, and A. P. Horsfield, (2010), submitted to J. Chem. Phys. (2010), submitted to J. Chem. Phys.